

Gas-based detectors for synchrotron radiation

Graham C. Smith

 Instrumentation Division, Brookhaven National Laboratory, Upton, NY 11973-5000, USA.
 E-mail: gsmith@bnl.gov

 Received 21 June 2005
 Accepted 19 October 2005

Gas-filled detectors have played an important role in experiments at synchrotron sources for many years. Although other X-ray detection technologies are gaining wider use, particularly with the higher flux of new sources, gas-filled detectors are still well suited for specific experiments. This article describes some fundamental characteristics of gas-filled detectors for X-ray detection, with emphasis on position encoding, position resolution and linearity. Recently developed micropattern structures for achieving electron multiplication are described. Some applications of conventional wire chambers and micro-pattern detectors are given.

 © 2006 International Union of Crystallography
 Printed in Great Britain – all rights reserved

Keywords: X-ray detectors; proportional chamber; position sensing; position resolution.

1. Introduction

Gas-filled detectors, in a variety of forms and operating with some level of electron gain, have been used as X-ray converters and position-encoding instruments since the very first synchrotron experiments were carried out. Over this approximately 30 year period, they have at various times been the mainstay detector in specific classes of experiment, sometimes to be superseded later by a more appropriate and generally commercially produced device. A classic example is in X-ray protein crystallography, where in the 1980s two-dimensional multi-wire chambers (MWPCs) were found on many of these beamlines (Phizackerley *et al.*, 1986). At that time they competed with TV detectors (Arndt, 1984), but both were progressively replaced by the image plate (Amemiya *et al.*, 1988) and then the scintillator/CCD (Gruner & Ealick, 1995) as the *de facto* protein crystallography detector. The driving force in this class of experiment has always been, primarily, higher count rate and better position resolution. While the MWPC has been unable to match the capabilities of more recent detectors for this application, its inherent properties, and those of later gas-filled devices based on micro-pattern detectors, provide synchrotron users in a wide range of other experiments with capabilities that are, still, unattainable with other detector types. Wide-angle and small-angle X-ray scattering (WAXS, SAXS) and studies with weak signals in a diffuse background (*e.g.* speckle) are three such fields where gas-filled detectors are almost indispensable. This article will illustrate some of their key characteristics.

2. Some fundamental properties

2.1. Efficiency

One of the most basic properties is X-ray stopping power. Because of their low operating voltages compared with

complex molecules, and their inherent stability, argon, krypton and xenon are the main constituents used in gas-filled detectors, together with a small volume (of order 10%) of quench gas, used to prevent the electron avalanche from becoming self-sustaining. The absorption depth (in which 63% of incoming photons are absorbed) in each of these noble gases is shown in Fig. 1, calculated from measured X-ray cross-section data (Storm & Israel, 1970). Because it has the highest atomic number, xenon has the greatest stopping power. In general, good stopping power can be achieved with argon in the X-ray range 3–8 keV, and with xenon in the range 8–40 keV. Krypton has slightly better stopping power than xenon in the range between their respective *K*-edges, 14.3–34.6 keV. These properties can be useful in choosing a suitable gas for an experiment if cost is a serious constraint (xenon about \$10 per liter, krypton about \$3 per liter, and argon is much cheaper than both). Exact conversion efficiencies can be easily evaluated for specific gas mixtures with the use of web tools, for example the Lawrence Berkeley Laboratory on-line calculator

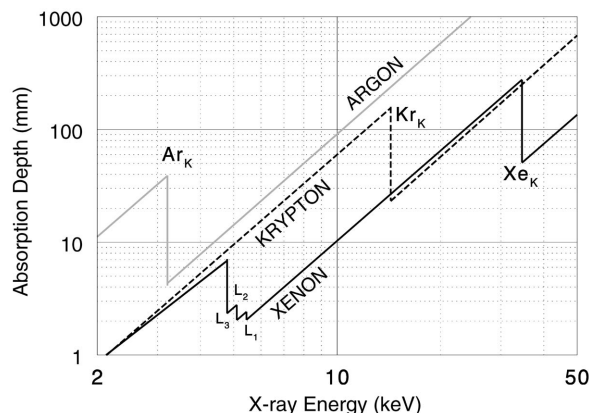


Figure 1
Absorption depth as a function of X-ray energy.

for photon transmission/absorption (http://www.cxro.lbl.gov/optical_constants/gastrn2.html).

2.2. Position resolution

Position resolution, σ_{det} , is determined by several factors. In non-pixelated detectors, it is generally determined by four main contributors,

$$\sigma_{\text{det}} = (\sigma_{\text{noise}} + \sigma_{\text{diff}} + \sigma_{\text{er}} + \sigma_{\text{aval}})^{1/2}, \quad (1)$$

where σ_{noise} is the r.m.s. contribution from electronic noise, σ_{diff} the contribution from electron diffusion, σ_{er} the contribution from photoelectron and Auger electron range and σ_{aval} the contribution from avalanche centroid fluctuation. The effect of parallax is not considered here, and will be described in a later section. σ_{noise} is dependent upon the type of readout and will not be quantified at this point. σ_{diff} is generally the smallest of the three contributors. σ_{er} is the parameter that can be quantified independent of detector type. σ_{aval} derives from statistical variations in the electron avalanche centroid, which is also dependent upon detector type, and greatly dependent upon gas gain; in practice, it can be easily the major contributor, and is probably the least considered phenomenon in gas detector operation. Here we will focus on σ_{er} , the results based largely on three sets of measurements (Fischer *et al.*, 1986a,b; Smith *et al.*, 1994) in which the detector and its mode of operation ensured that all but σ_{er} in equation (1) were negligible. A synopsis of these ‘electron range limited’ position-resolution measurements, all at 10^5 Pa operating pressure, is shown in Fig. 2. Several generalizations can be made. In the X-ray energy range 3.2–6 keV, argon provides the capability of 100 μm resolution. In the X-ray energy range 6–10 keV, xenon provides the capability of 100 μm resolution. In the 10–15 keV region, xenon achieves a resolution that increases from 100 μm to 300 μm . In the 15–20 keV region, gating on the Kr_K escape peaks can yield resolution ranging from <100 μm to 200 μm . The region 20–34.6 keV is totally dominated by long-range effects of photoelectrons in both Kr and Xe, but there is a dramatic improvement above the Xe_K edge. In the range 34.6–45 keV, gating on Xe_K escape peak events provides resolution from 100 μm to 350 μm . Taken in conjunction with efficiency curves in Fig. 1, a user requiring a specific position

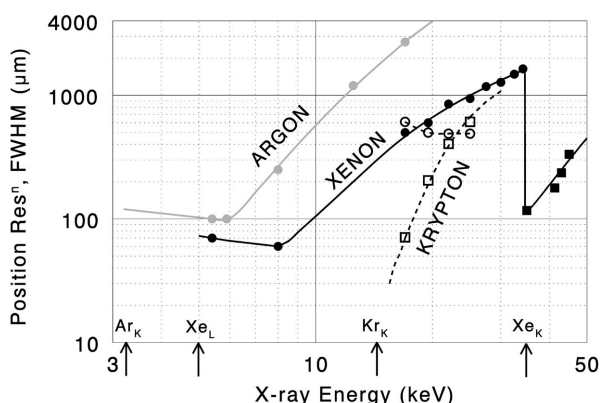


Figure 2 Position resolution at 10^5 Pa (with 10% quench gas).

resolution can make an empirical choice of gas mixture to suit the energy requirements of the experiment.

2.3. Counting rate (limitation owing to space charge)

One of the first models for describing the electric field reduction at an anode wire surface, owing to positive-ion space charge, was given by Sipila *et al.* (1980). This was followed by a more comprehensive description that accounted for second-order effects such as anode wire diameter (Mathieson & Smith, 1992). The presence of any positive ions in the volume between anode and cathode will cause an effective reduction in the electric field at the anode surface, and hence there is a decrease in the gas gain. This model calculates the effective field reduction and excellent agreement was obtained between prediction and measurement. An example of the predicted avalanche size *versus* count rate for a specific detector geometry is shown in Fig. 3. Since avalanche size (in the absence of major charge saturation) is the product of primary charge and gas gain, higher count rates will be sustained with lower gas gain. Lower gas gain will also prolong the onset of aging effects, in which deposits are formed on the anode electrode and another, independent, reduction in gas gain occurs. A thorough analysis of this ‘aging’ phenomenon was given by Kadyk (1991) and more recently by Va’vra (2003) and Sauli (2003).

3. Basis of conventional position encoding

In the majority of gas-filled detectors, the basis of both one- and two-dimensional X-ray encoding is determination of the centroid of cathode charge, induced from an anode avalanche. Fig. 4 shows that the footprint of charge on the cathodes is significant, compared with the small (<1 mm) physical extent of the anode avalanche. In fact the induced cathode charge has a quasi-Gaussian profile with a FWHM of about $1.6d$, where d is the anode–cathode spacing (Gatti *et al.*, 1979; Gordon & Mathieson, 1984). In practice, readouts for cathodes have been developed that essentially determine the centroid of charge on the strips/wires, a measurement that yields a precision much better than the strip pitch. The most common readout techniques are delay line, or amplifier per strip/wire. In general, delay-line readout achieves 10^5 to 10^6 counts s^{-1} , and advanced examples of amplifier per strip can achieve 10^7 counts s^{-1} and a little beyond.

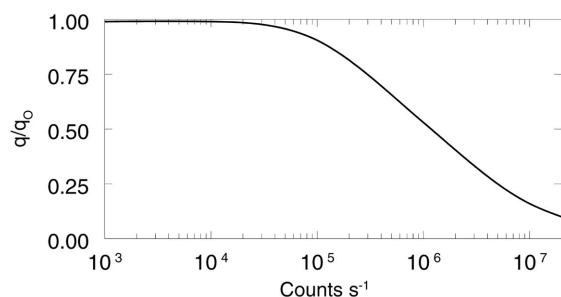


Figure 3 Relative drop in gain *versus* count rate.

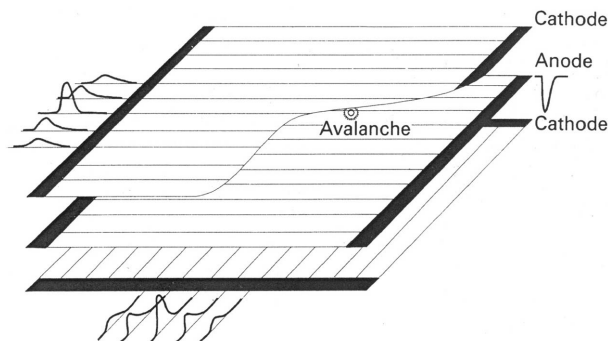


Figure 4
Cathode-induced charge from an anode avalanche.

4. Delay-line detectors

4.1. General operation

Position readout with delay line represents the most highly developed, and most frequently used, encoding system for X-ray synchrotron experiments (Smith *et al.*, 1992). Their robust and excellent performance in terms of resolution and linearity have long been known (Boie *et al.*, 1982). With this readout, all cathode strips/wires feed the nodes of a delay line, and timing information of the signals at each end of the line determines the centroid location. Fig. 5 shows the principle. The classic calibration measurement with such a system is determination of X-ray position resolution as a function of anode charge, as shown in Fig. 6 (Capel *et al.*, 1995). This illustrates that, as the anode charge is increased, position resolution, at first, improves as the reciprocal of the anode charge. This corresponds to detector operation in a regime where the electronic noise contribution, σ_{noise} , is dominant. As anode charge is increased, the resolution begins to deviate from the 45° line, because other factors, primarily electron range, become significant. However, if the anode signal is increased too much, the resolution begins to deteriorate, a mode of operation to be avoided because the avalanche begins to spread along the wire, contributing to an increasing value of σ_{aval} . This diagram also illustrates the effect of changing delay-line transit time. In this example, reducing the transit time from 1 μs to 0.5 μs , the electronic noise (which in terms of

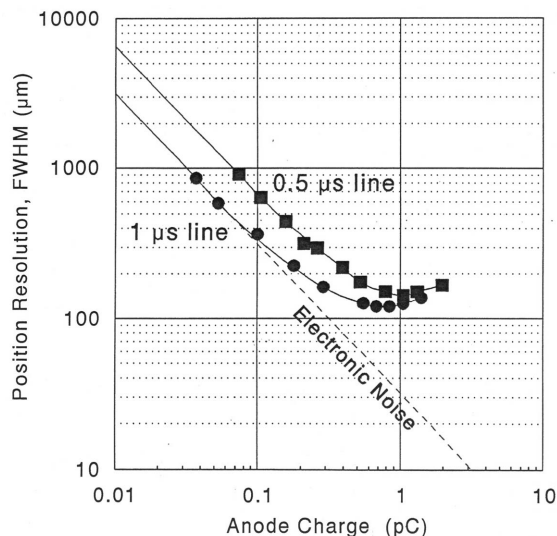


Figure 6
Position resolution (FWHM, μm) versus anode charge.

number of electrons remains virtually the same) has increased its contribution, σ_{noise} , by a factor of two because the time scale over which position is determined has been halved, while the absolute uncertainty in timing at each end of the delay line remains essentially unchanged.

4.2. Time-to-digital converter

Timing information from the delay line is converted into position by a time-to-digital converter (TDC), which is one of the most crucial elements in a correctly operational instrument. Excellent differential non-linearity is a key desired characteristic, and few really good TDCs have been developed specifically for delay-line detectors. Some examples over the last 15 years are given by Harder (1988), Berry (1993), Chemloul & Comparat (1995), Epstein & Boulin (1998), Hervé & Le Caër (1999) and Levchanovski *et al.* (2004). It is probably true to say that the ready availability of a quality TDC containing the proper discriminators would have contributed significantly to efficient use of delay-line detectors in the synchrotron environment. While the examples cited

have helped tremendously in this respect, appropriate TDCs are in general not available in great numbers or commercially. Two important discriminator functions were incorporated into one of the first TDC developments (Harder, 1988). The first, and most important, is the sum discriminator. With reference to Fig. 5, this discriminator ensures that the sum of the left scaler and right scaler contents, for a single event, is equal to the delay-line transit time, τ . If this condition is not met, all events relating to those timing signals are aborted. The response of this TDC to an electronic input that simu-

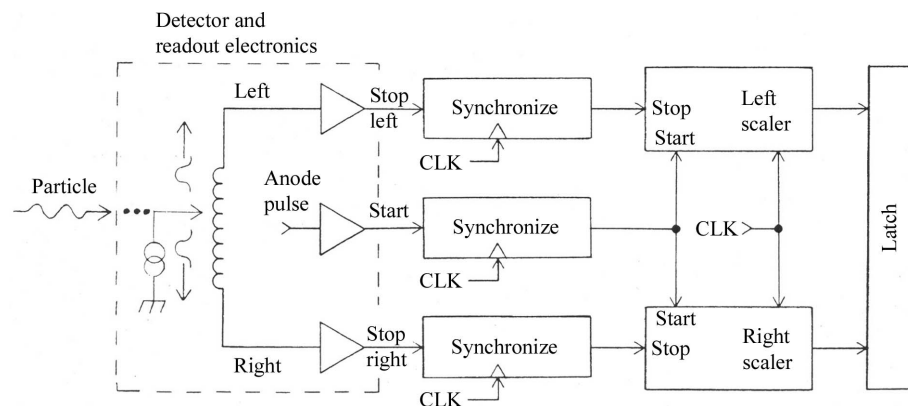


Figure 5
Front-end synopsis of delay-line readout (one-axis only shown).

lates, accurately, all positions, is shown in Fig. 7(a). The differential non-linearity is $<0.1\%$, an excellent value. When the TDC is connected to a (one-dimensional) delay-line detector ($\tau = 1 \mu\text{s}$) which is illuminated with X-rays, the uniform irradiation response (UIR) at $20 \times 10^3 \text{ counts s}^{-1}$ is shown in Fig. 7(b). This illustrates the good linearity of the detector in terms of uniform conversion per unit length and uniformity of delay-line response. If the sum discriminator is not incorporated, then at high rate a peaked response is generated, as shown by the UIR at $10^6 \text{ counts s}^{-1}$ shown in Fig. 7(c). This occurs because of a tendency for the left and

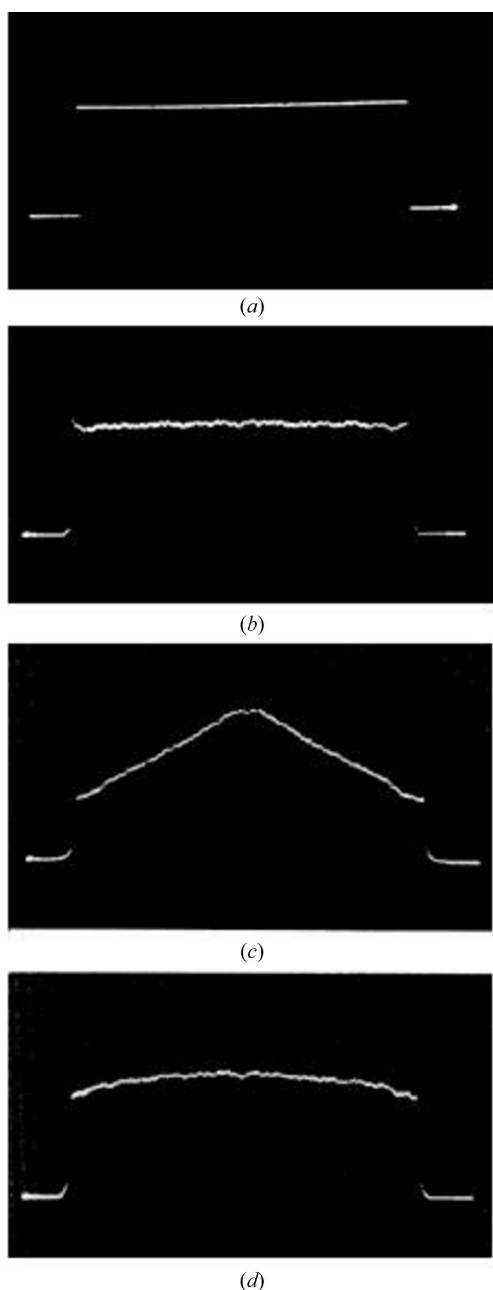


Figure 7
Uniform irradiation responses (UIRs) using purpose-designed TDC. (a) Electronic calibration, intrinsic non-linearity $<0.1\%$. (b) $20 \times 10^3 \text{ counts s}^{-1}$, no discriminators. (c) $10^6 \text{ counts s}^{-1}$, no discriminators. (d) $10^6 \text{ counts s}^{-1}$, with sum discriminator.

right scaler to be stopped close together in time, thereby simulating an event toward the center of the detector. An unusual, and at first surprising, second-order artifact occurs when the sum discriminator is applied at high rate, as shown in Fig. 7(d): there is still a small excess of events at the center of the detector. There is, in fact, a position dependency to the events that are rejected: an event at either end of the delay line will generate one signal that takes almost τ to reach the end of the delay line, while signals for an event in the center will take only $\tau/2$ to reach each end of the line. Therefore, events at the edge of the detector are more likely to be rejected through the occurrence of the next event than those in the center. Application of a ‘minimum inter-arrival time’ discriminator generates a flat spectrum very similar to that in Fig. 7(b), at the expense of throughput. The latest TDC development (Levchanovski *et al.*, 2004) includes logic to try and disentangle signals from more than one event to improve throughput at high rates.

4.3. Linearity

An application that is ideally suited to the low background sensitivity of a gas-filled detector is measurement of speckle. This has been described by Kocsis (1997). At Brookhaven’s National Synchrotron Light Source, an improved version of a detector (Smith & Yu, 1995), with wire and electrode spacing less than 1 mm, is under study for speckle measurements (Dierker & Shin, 2004). It possesses extremely good position resolution and linearity in both axes, as shown by the image of a 15 mm-diameter plastic gear wheel in Fig. 8, and, with $3 \times 10^5 \text{ Pa}$ of xenon, can achieve a resolution of about $50 \mu\text{m}$.

5. Micro-pattern detectors

A number of detectors in which electron multiplication takes place in high field regions around lithographically produced anodes have been developed over the last 15 years. Among other features, these offer the hope that gas-filled detectors can be fabricated more automatically, with much less of the labor-intensive effort required for MWPCs. While not an exhaustive list, some of these devices are the micro-strip gas chamber, MSGC (Oed, 1988), the micro-gap chamber,

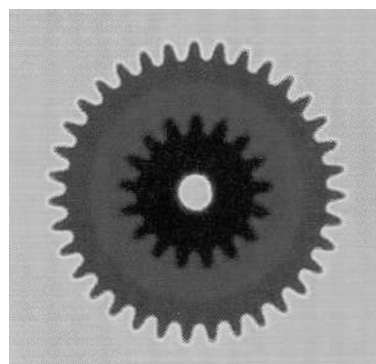


Figure 8
Example of good linearity in both axes of an MWPC (transmission image of a 1.5 cm-diameter gear wheel).

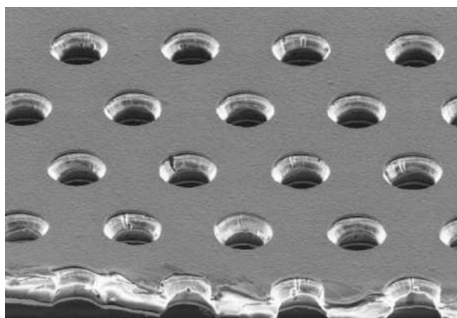


Figure 9
Example of a gas electron multiplier (GEM), etched from Cu-coated kapton. The diameter of the holes is about 75 μm .

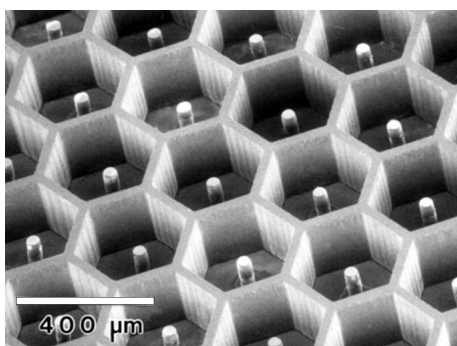


Figure 10
Micro-pin array (MIPA). Anode pin spacing is 400 μm .

MGC (Bellazzini & Spandre, 1995), the compteur a trous, CAT (Bartol *et al.*, 1996), the gas electron multiplier, GEM (Sauli, 1997), the micro-mesh-gaseous structure, Micromegas (Giomataris *et al.*, 1996) and micro-pin array, MIPA (Rehak *et al.*, 1997). Photographs of a part of a GEM structure, and part of a MIPA structure, are shown in Figs. 9 and 10, respectively.

6. Further developments

Developments have taken place at a number of synchrotron sources aimed at improving the count-rate capability of two-dimensional detectors. We will describe three that have achieved significant application in synchrotron experiments.

6.1. Amplifier per wire in a MWPC

A development over the last few years at Daresbury Laboratory has resulted in an instrument known as the RAPID (refined ADC per input detector) system. RAPID1 (Lewis *et al.*, 1997) evolved into a 20 cm \times 20 cm micro-gap detector with 256 wires/strips on each x, y readout axis, achieved with 128 readout channels per axis. Each readout channel comprises a preamplifier, ADC, with wire/strip digital information used to calculate a center-of-gravity for each event. A schematic of the micro-gap format is shown in Fig. 11. A combination of shorter positive-ion collection time, short shaping time, and a degree of parallelism in the analysis permits this system to sustain counting rates that are in excess

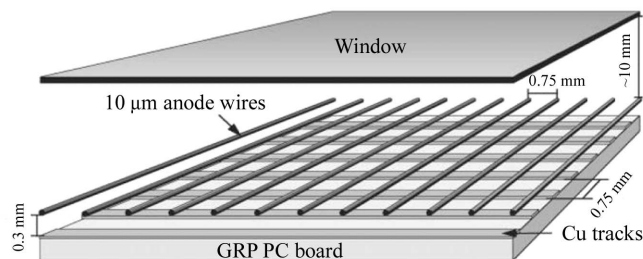


Figure 11
Concept of the micro-gap chamber.

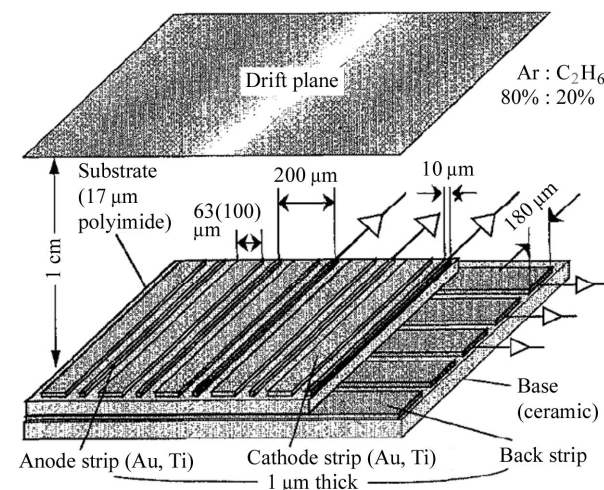


Figure 12
MSGC with two-dimensional readout.

of standard delay-line readout. Global count rates of $2 \times 10^7 \text{ s}^{-1}$, local (single diffraction peak) count rates of 10^6 s^{-1} , and a position resolution of about 300 μm FWHM have been reported. RAPID2 (Berry *et al.*, 2003) is a second-generation system consisting of a curved detector and an improved algorithm/faster RAM.

6.2. Amplifier per wire in a MSGC

Significant development in MSGCs has taken place in Japan. A two-dimensional detector was produced on a thin substrate, with the second coordinate determined from cross-strips separated from the front surface by a 17 μm polyimide spacer. The principle is shown in Fig. 12 (Tanimori *et al.*, 1996). Improved larger versions of this early device have been used at Spring-8 SAXS experiments (Toyokawa *et al.*, 2001). Further, advanced micro-pattern detector developments are under way also in Japan (Ochi *et al.*, 2002; Takahashi *et al.*, 2003).

6.3. CAT- and GEM-based detectors

At Synchrotron Trieste, advances have been achieved using the CAT. This features a gas amplifying micro-hole structure in combination with a resistive position-encoding structure, the latter divided into small independent elements (Sarvestani *et al.*, 1998). A schematic diagram of a small part of the

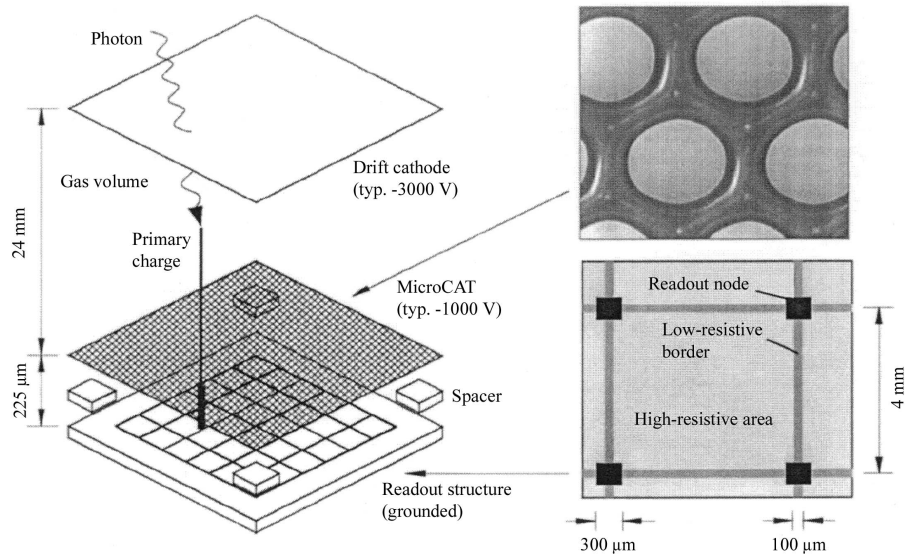


Figure 13
Principle of the MicroCAT detector.

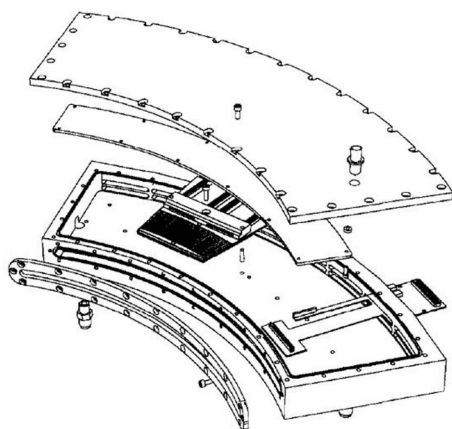


Figure 14
One-dimensional detector with radial readout, and no parallax error.

detector structure is shown in Fig. 13. X-rays convert as usual, between the window and MicroCAT electrode, and primary electrons multiply in the small gap between the MicroCAT and the readout structure. As shown at the bottom right, the readout structure is divided into square resistive pads, with a readout node at each corner; measurement of the signal charge at each corner will permit localization of the center-of-gravity of the event to a fraction of the 4 mm side. The method of multiple readout, and recent developments regarding replacement of the MicroCAT with GEMs, are described by Orthen *et al.* (2004).

7. Parallax reduction

7.1. One-dimensional encoding

The conventional approach to eliminating parallax errors in one dimension is to construct the conversion depth of the detector with an appropriate radius of curvature. This is quite impossible in the case of a wire detector, with the wire

direction along the sensing axis. Alternative electron multiplying technologies have been adopted to resolve this, such as a blade (Ballou *et al.*, 1983; Yu *et al.*, 1998), in which multiplication occurs along the sharp edge of a metal blade or sheet, and which can be fabricated as an arc. A method that permitted off-line correction of parallax by determination of the depth at which X-ray conversion occurred in a planar slab of gas was demonstrated with a multi-step avalanche chamber (Bateman *et al.*, 1985). None of these approaches have been adopted in a serious way at synchrotron sources, although curved detectors are available commercially (<http://www.inel.fr/en/contact/>) using a blade operating in the limited streamer mode, with generally restricted rate and resolution capability.

The conventional geometry for operating MWPCs and most micro-pattern detectors in X-ray scattering experiments requires photons to enter the detector in a direction perpendicular to the planes of the electrodes. All X-rays converted at a specific x, y location create primary electrons that drift to the same location for multiplication. This situation leads to the phenomenon of space charge saturation, outlined earlier, in which the local electric field strength is reduced and the gas gain is also reduced.

A method that largely eliminates the space charge problem, and also eliminates parallax errors, is to permit X-rays to enter the detector such that their trajectory is parallel to the electron multiplying plane. Applicable only as a one-dimensional device, this approach is well suited to the MSGC, and Fig. 14 shows the principle. This mode of operation has been developed at the European Synchrotron Radiation Facility (Zhukov *et al.*, 1997) and at the Rutherford Appleton Laboratory (Bateman *et al.*, 2002).

7.2. Two-dimensional encoding

Only a few years after the initial concept of the MWPC had been developed, Charpak's group at CERN studied the possibility of adding a spherical drift chamber to the front of a conventional planar MWPC (Charpak *et al.*, 1974). This scheme was mechanically challenging, but a working device was developed for the LURE synchrotron source in the 1980s (Kahn *et al.*, 1986) as a workhorse for a number of years. More recently, the mechanical difficulties associated with the latter approach were removed by adapting the electric field in an existing planar detector to exhibit a quasi-spherical field (Rehak *et al.*, 1997). A comparison of the normal field, and modified field, of this arrangement is shown in Fig. 15. The much improved position resolution of this scheme is shown in Fig. 16, in which a 5.4 keV beam is incident on a planar detector containing Xe/10%-CO₂ at angles from zero to 12°.

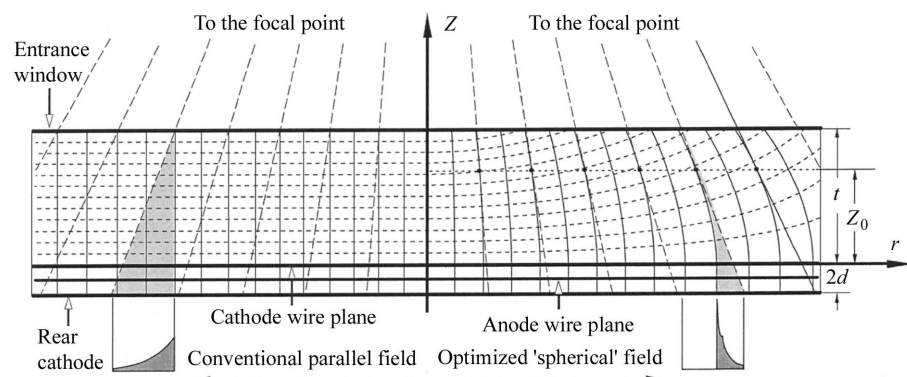


Figure 15
Principle of parallax reduction in a planar detector.

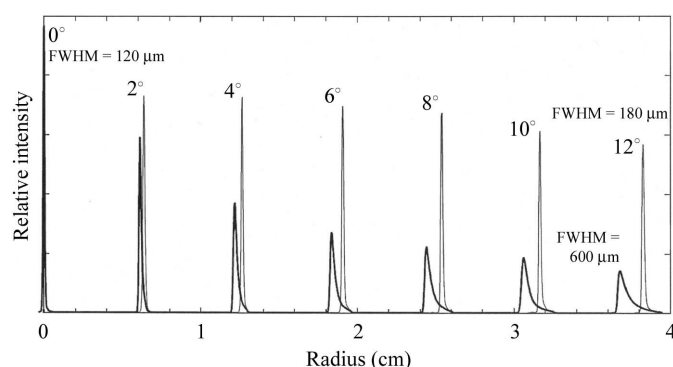


Figure 16
Position-resolution measurements without (thick lines) and with (thin lines) parallax reduction. Collimated 5.4 keV X-rays, Xe/10%-CO₂.

The improvement in FWHM is very significant. This scheme has not been adopted in a significant way as yet; the Daresbury Laboratory is studying an application (Helsby, 2004) and the Institute Laue Langevin is investigating the technique for application to neutron detectors (Van Esch *et al.*, 2005).

8. Conclusion

Gas-filled detectors can provide efficient high-resolution high-rate detection of X-rays. They have extremely low background, and in many applications provide a cost-effective solution that is unattainable with any other device. While they are considered a mature instrument, new developments in operation of wire chambers and innovative methods for electron multiplication in a gas are occurring. It appears likely that these detectors will continue to find useful application in synchrotron experiments in the foreseeable future.

The development work and results presented here reflect the efforts of many research groups and collaborators. The author is indebted to colleagues working in the field of gas detectors for many informative and enjoyable discussions. This work was supported by the United States Department of Energy under Contract No. DE-AC02-98CH10886.

References

- Amemiya, Y., Matsushita, T., Nakagawa, A., Satow, Y., Miyahara, J. & Chikawa, J. (1988). *Nucl. Instrum. Methods*, **A266**, 645–653.
- Arndt, U. W. (1984). *Nucl. Instrum. Methods*, **222**, 252–255.
- Ballou, J., Comparat, V. & Poux, J. (1983). *Nucl. Instrum. Methods*, **217**, 213–216.
- Bartol, F., Bordessoule, M., Chaplier, G., Lemonnier, M. & Megtert, S. (1996). *J. Phys. III Fr.* **6**, 337–347.
- Bateman, J. E., Connelly, J. F., Derbyshire, G. E., Duxbury, D. M., Lipp, J., Mir, J. A., Simmons, J. E., Spill, E. J., Stephenson, R., Dobson, B. R., Farrow, R. C., Helsby, W. I., Mutikainen, R. & Suni, I. (2002). *Nucl. Instrum. Methods*, **A477**, 340–346.
- Bateman, J. E., Connolly, J. F. & Stephenson, R. (1985). *Nucl. Instrum. Methods*, **A239**, 251–259.
- Bellazzini, R. & Spandre, G. (1995). *Nucl. Instrum. Methods*, **A368**, 259–264.
- Berry, A. (1993). *Rev. Sci. Instrum.* **64**, 1222–1228.
- Berry, A., Helsby, W. I., Parker, B. T., Hall, C. J., Buksh, P. A., Hill, A., Clague, N., Hillon, M., Corbett, G., Clifford, P., Tidbury, A., Lewis, R. A., Cernik, B. J., Barnes, P. & Derbyshire, G. E. (2003). *Nucl. Instrum. Methods*, **A513**, 260–263.
- Boie, R. A., Fischer, J., Inagaki, Y., Merritt, F. C., Radeka, V., Rogers, L. C. & Xi, D. M. (1982). *Nucl. Instrum. Methods*, **201**, 93–115.
- Capel, M. S., Smith, G. C. & Yu, B. (1995). *Rev. Sci. Instrum.* **66**, 2295–2299.
- Charpak, G., Hajduk, Z., Jeavons, A., Stubbs, R. J. & Kahn, R. (1974). *Nucl. Instrum. Methods*, **122**, 307.
- Chemloul, M. & Comparat, V. (1995). *Nucl. Instrum. Methods*, **A355**, 532–536.
- Dierker, S. & Shin, T. J. (2004). Private communication.
- Epstein, A. & Boulin, C. (1998). *IEEE Trans. Nucl. Sci.* **NS-45**, 1931–1933.
- Fischer, J., Radeka, V. & Smith, G. C. (1986a). *Nucl. Instrum. Methods*, **A252**, 239–245.
- Fischer, J., Radeka, V. & Smith, G. C. (1986b). *IEEE Tran. Nucl. Sci.* **NS-33**, 257–260.
- Gatti, E., Longoni, A., Okuno, H. & Semenza, P. (1979). *Nucl. Instrum. Methods*, **163**, 83–92.
- Giomataris, Y., Rebourgeard, Ph., Robert, J. P. & Charpak, G. (1996). *Nucl. Instrum. Methods*, **A376**, 29–35.
- Gordon, J. S. & Mathieson, E. (1984). *Nucl. Instrum. Methods*, **227**, 267–276.
- Gruner, S. M. & Ealick, S. E. (1995). *Structure*, **3**, 13–15.
- Harder, J. A. (1988). *Nucl. Instrum. Methods*, **A265**, 500–510.
- Helsby, W. (2004). Private communication.
- Hervé, C. & Le Caër, T. (1999). *Rev. Sci. Instrum.* **70**, 226–231.
- Kadyk, J. (1991). *Nucl. Instrum. Methods*, **A300**, 436–479.
- Kahn, R., Fourme, R., Bosshard, R. & Saintagne, V. (1986). *Nucl. Instrum. Methods*, **A246**, 596–603.
- Kocsis, M. (1997). *Nucl. Instrum. Methods*, **A392**, 28–31.
- Levchanovski, F. V., Gebauer, B., Litvinenko, E. I., Nikiforov, A. S., Prikhodko, V. I., Schulz, Ch. & Wilpert, Th. (2004). *Nucl. Instrum. Methods*, **A529**, 413–416.
- Lewis, R. A., Helsby, W. I., Jones, A. O., Hall, C. J., Parker, B., Sheldon, J., Clifford, P., Hillem, M., Sumner, I., Fore, N. S., Jones, R. W. M. & Roberts, K. M. (1997). *Nucl. Instrum. Methods*, **A392**, 32–41.
- Mathieson, E. & Smith, G. C. (1992). *Nucl. Instrum. Methods*, **A316**, 246–251.
- Ochi, A., Nagayoshi, T., Koishi, S., Tanimori, T., Nagae, T. & Nakamura, M. (2002). *Nucl. Instrum. Methods*, **A478**, 196–199.

- Oed, A. (1988). *Nucl. Instrum. Methods*, **A263**, 351–359.
- Orthen, A., Wagner, H., Martoiu, S., Amenitsch, H., Bernstorff, S., Besch, H. J., Menk, R. H., Nurdan, K., Rappolt, M., Walenta, A. H. & Werthenbach, U. (2004). *J. Synchrotron Rad.* **11**, 177–186.
- Phizackerley, R. P., Cork, C. W. & Merritt, E. A. (1986). *Nucl. Instrum. Methods*, **A246**, 579–595.
- Rehak, P., Smith, G. C. & Yu, B. (1997). *IEEE Trans. Nucl. Sci.* **NS-44**, 651–655.
- Sarvestani, A., Besch, H. J., Junk, M., Meißner, W., Sauer, N., Stiehler, R., Walenta, A. H. & Menk, R. H. (1998). *Nucl. Instrum. Methods*, **A410**, 238–258.
- Sauli, F. (1997). *Nucl. Instrum. Methods*, **A386**, 531–534.
- Sauli, F. (2003). *Nucl. Instrum. Methods*, **A515**, 358–363.
- Sipila, H., Vanha-Honko, V. & Bergqvist, J. (1980). *Nucl. Instrum. Methods*, **176**, 381–387.
- Smith, G. C., Cox, D. E. & Jephcoat, A. P. (1994). *Nucl. Instrum. Methods*, **A350**, 621–623.
- Smith, G. C. & Yu, B. (1995). *IEEE Trans. Nucl. Sci.* **NS-42**, 541–547.
- Smith, G. C., Yu, B., Fischer, J., Radeka, V. & Harder, J. A. (1992). *Nucl. Instrum. Methods*, **A323**, 78–85.
- Storm, E. & Israel, H. I. (1970). *Nucl. Data Tables*, **A7**, 565–681.
- Takahashi, H., Hagai, C., Yano, K., Fukuda, D., Nakazawa, M., Kishimoto, S., Ino, T., Furusaka, M. & Hasegawa, K. (2003). *Nucl. Instrum. Methods*, **A410**, 238–258.
- Tanimori, T., Ochi, A., Minami, S. & Nagae, T. (1996). *Nucl. Instrum. Methods*, **A381**, 280–288.
- Toyokawa, H., Fujisawa, T., Inoko, Y., Nagayoshi, T., Nishi, Y., Nishikawa, Y., Ochi, A., Suzuki, M. & Tanimori, T. (2001). *Nucl. Instrum. Methods*, **A467–468**, 1144–1147.
- Van Esch, P., Clergeau, J. F. & Medjoubi, K. (2005). *Nucl. Instrum. Methods*, **A540**, 361–367.
- Va'vra, J. (2003). *Nucl. Instrum. Methods*, **A515**, 1–14.
- Yu, B., Smith, G. C., Siddons, D. P. & Pietraski, P. J. (1998). *Nucl. Instrum. Methods*, **A419**, 519–524.
- Zhukov, V., Udo, F., Marchena, O., Hartjes, F. G., van den Berg, F. D., Bras, W. & Vlieg, E. (1997). *Nucl. Instrum. Methods*, **A392**, 83–88.